ISSN 0915-633X

NIFS—266

JP9404098

A Research of Possibility for Negative Muon Production by a Low Energy Electron Beam Accompanying Ion Beam

J. Uramoto

(Received – Nov. 1, 1993)

NIFS-266 Dec. 1993

A research of possibility for negative muon production by a low energy electron beam accompanying ion beam

Jôshin URAMOTO

National Institute of Fusion Science, Nagoya 464-01, JAPAN

Keywords: negative muonlike particle, bunched beam electron, positive ion beam

Abstract

A low energy electron beam (≤ 2000 eV) is injected perpendicularly to a uniform magnetic field, together with a low energy positive ion beam. On this magnetic mass analysis (using the uniform magnetic field), a peak of secondary electron current to the beam collector (arranging as a mass analyzer of 90° type), appears at an analyzing magnetic field which corresponds exactly to a relation of negative muon μ^- (the mass $m = 207\, m_e$ and the charge $q = e$, where m_e and e are mass and charge of electron). The ion beam is essential for the peak appearance, which is produced by decelerating electrically the electron beam in front of the entrance slit of the mass analyzer, and by introducing a neutral gas into the electron beam region and producing a plasma through the ionization. We consider that a very small amount of negative muons may be produced through local cyclotron motions of the injected beam electrons in the ion beam or by an interaction between the bunched beam electrons and beam ions.

As one of nuclear fusions using D_2 and T_2, the negative muon μ^- catalyzed fusion is one possible method.[1] However, up to now, the negative muon μ^- has been produced only through a decay of π meson produced by some high energy particle accelerators above an energy of a few 100 MeV. Therefore, even if the negative muon catalyzed fusion succeeds physically, it's industrial application is not hopeful in efficiency and in simplicity. Then, it is very important to research simple and efficient possibilities of the negative muon production.

At the starting point of this research, we noted that physical characters of negative muon μ^- are similar to those of electron e except for mass, and that a localized injection of energetic electrons in a positive ion beam may produce "some resonance state" among their electrons through a transfer of energy from the ion beam. Under these considerations, an electron beam will be injected perpendicularly to a weak uniform magnetic field while an positive ion beam is also injected together with the electron beam. Then, two experimental methods to inject both an electron beam and an positive ion beam, will be shown. It should be noted that a magnetic mass analyzer is utilized to generate the uniform magnetic field, and that the analyzing beam

collector is biased positively with respect to the mass analyzer body in order to detect negatively charged particles.

Schematic diagrams of the first experimental apparatus are shown in Fig. 1 and Fig. 2. The initial or first electron beam (F.E.B.) is stopped critically in front of the entrance slit S by an electrical potential of the decelerator D connected to the cathode of the electron gun. Next, a neutral gas is introduced into the first electron beam region and a plasma is produced through ionization of the gas. Then, ions of the plasma are accelerated in front of S while an ion beam with an energy corresponding to the first electron beam acceleration voltage V_A, is injected into the magnetic field region through S. Moreover, the stopped beam electrons are reaccelerated electrically toward the gap between two magnetic poles (N) and (S) through S, while the injected ion beam is decelerated electrically and stopped in the gap. The electrically reaccelerated electrons are injected perpendicularly to the magnetic field (B_M) and bunched in cyclotron motions of small radius.

As shown in Fig. 2, the above magnetic system is used as a mass analyzer (M.A.) of 90° type when the beam collector B.C. is arranged. The analyzing curvature radius r is 4.3 cm. It should be noted that the bias voltage V_S of the beam collector is positive with respect to the mass analyzer in order to reject an ion current and draw back the secondary electrons.

A fringe magnetic field distribution of the analyzing magnetic field B_M under a magnetic coil current of 1A, is shown in Fig. 3 for two different metal plates as the entrance plate (decelerator D) of Fig. 1 and Fig. 2. In this experiment, the iron (Fe) plate is used and the fringe magnetic field is much reduced.

Dependences of negative current I^- to the beam collector B.C. on the analyzing magnetic field B_M are shown in Fig. 4 for various first electron beam acceleration voltage V_A under a basic pressure (air) of 5×10^{-6} Torr in the first electron beam region. Here, we find that an analyzing relation of the negative muonlike particle $\mathring{\mu}^-$ is satisfied for each peak of negative current I^-, assuming that the effective acceleration voltage V_E is twice of the first electron beam acceleration voltage V_A. That is, the following relation is found by

$$r = \frac{48\sqrt{V_E}}{B_M}$$

$$V_E = 2\,V_A, \quad \text{..... (1)}$$

where r (the analyzing curvature radius = 4.3 cm) is in cm unit, B_M (an analyzing magnetic field where each negative current I^- shows a peak value) is in gauss unit and V_E (an effective acceleration voltage of the negative muonlike particle) is in V (volt) unit.

Generally, from the analyzing magnetic field B_M under the curvature radius r of the mass analyzer, where the negative current shows a peak, and the effective acceleration voltage V_E, we can estimate the mass m of the negatively charged particle by,

$$m = \frac{e\,(B_M r)^2\, m_e}{2V_E}$$

$$= \frac{8.8 \times 10^{-2}\,(B_M r)^2\, m_e}{V_E}, \quad \text{..... (2)}$$

where e is the electron charge, B_M is in gauss unit, r is in cm unit, V_E is in volt unit and m_e is the electron mass. For the curvature radius r = 4.3 cm of this mass analyzer, the Eq. (2) is rewritten by

$$m = \frac{1.63\,B_M^2}{V_E}\, m_e. \quad \text{..... (3)}$$

Thus, from the experimental conditions in Fig. 4, we obtain $m = 200 \sim 208\ m_e$ for $V_E = 2\,V_A$.

We assume "a negative muonlike particle" $\mathring{\mu}^-$ to explain the peak corresponding to the relation of Eq. (1) or Eq. (3). However, this assumption for $\mathring{\mu}^-$ does not mean that we detected the true muon μ^- as only the secondary electrons are observed as described later.

In order to compare an analyzing characteristic of negative muonlike particle $\mathring{\mu}^-$ with that of negative hydrogen ion H^-, we introduce H_2 gas into the first electron beam region.[2] Then, as shown in Fig. 5, we find another peak of the beam collector current I^- which corresponds to an analyzing relation of H^-. That is, the following relation is found, for the peak, by

$$r = \frac{144\sqrt{V_E}}{B_M}$$

$$V_E = 2\,V_A, \quad \text{..... (4)}$$

where r (the analyzing curvature radius = 4.3 cm) is in cm unit, B_M (an analyzing magnetic field) is in gauss unit and V_E (an effective acceleration voltage) is in V (volt) unit. These experimental facts show that both $\mathring{\mu}^-$ and H^- are accelerated by twice of V_A.

Next, we introduce He gas into the first electron beam region. Dependences of the beam collector current I^- on the analyzing magnetic field B_M are shown in Fig. 6 under a pressure of 1.5×10^{-4} Torr of He gas. Obviously, the peak of Fig. 5 corresponding to H^- is not found in Fig. 6. Each peak of I^- in Fig. 6 corresponds exactly to a relation of $\mathring{\mu}^-$ in Eq. (1).

A dependence of the beam collector current I^- on the bias voltage V_S with respect to the mass analyzer body (as seen in Fig. 1), is shown in Fig. 7 under the first electron beam acceleration voltage $V_A = 200V$. We find that the peak of negative current I^- saturates when V_S approaches to twice of V_A, ($V_E = 2\,V_A = 400V$). Similarly, a dependence of I^- on V_S is shown in Fig. 8 under $V_A = 1200V$, while I^- increases even if $V_S > 400V$ in comparison with that in a case of $V_A = 200V$.

A dependence of the beam collector current I^- on the total anode current I_A of the electron gun (as seen in Fig. 1), is shown in Fig. 9 under a Ar gas pressure of 1×10^{-4} Torr in the first electron beam region, $V_A = 400V$ and $V_S = 350V$. We find that the peak of I^- increases with I_A.

Finally, a dependence of the beam collector current I^- on the neutral gas (Ar) pressure P in the first electron beam region, is shown in Fig. 10 under $V_A = 400V$, $V_S = 350V$ and $I_A = 3$ mA. Similarly, we find that the peak of I^- increases with the pressure P while the peak of I^- saturates near $P \approx 2 \times 10^{-4}$ Torr.

For the experimental fact that the effective energy (V_E) of produced $\mathring{\mu}^-$ corresponds to $2\,V_A$, we consider that the $\mathring{\mu}^-$ particles are accelerated by both the applied voltage V_A (between the entrance slit S and the magnetic poles) and a potential of the stopped ion beam which is equal to V_A. Similarly, we consider that the H^- ions produced in the first electron beam region, are also accelerated by the two potentials.

To produce one negative true muon μ^- particle, an energy of $E_\mu = 105.7\ MeV$ or 1.7×10^{-11} Joule is required for the electron beam. Thus, a net current I_i^- (μA) of the produced true negative muons is estimated from an effective electron beam power W_{ef} (W) injected into the mass analyzer, if the kinetic energy of μ^- is neglected, by

$$I_i^- \approx \frac{eW_{ef}}{E_\mu}$$

$$= 9.4 \times 10^{-3}\ W_{ef}\ (\mu A), \quad \text{..... (5)}$$

At the productions of negative muonlike particles, we can estimate that the electron cyclotron radius is about $r_e \approx r/14 \approx 0.3$ cm when the $\mathring{\mu}^-$ particles arrive at the beam collector position $r = 4.3$ cm (an analyzing radius of the mass analyzer), because the peak of $\mathring{\mu}^-$ appears at a magnetic field 14 times larger that for the electron beam. Then, the number of times of the electron cyclotron motions are about 50 times, which are determined from $(1/4)\ (r/r_e)\ (v_e/v_\mu)$, where v_e and v_μ are the electron velocity and the negative muonlike particle velocity.

Here, if the cyclotron motions of about 50 times of the beam electrons inside the mass analyzer is considered as an energy multiplications due to a kind of confinement, Eq. (5) is rewritten by,

$$I_i^- \approx 4.7 \times 10^{-1}\ W_b\ (\mu A)$$

$$= 4.7 \times 10^{-7}\ I_b V_b\ (\mu A), \quad \text{..... (6)}$$

where W_b is an usual electron beam power (W unit), and I_b and V_b are the injected electron beam current (μA) and the effective electron beam acceleration voltage (V).

When the injected electron beam current is about 200 μA ~ 500 μA and the effective acceleration voltage is about 500V ~ 1000V, we obtain $I_i^- \approx 0.05\ \mu A \sim 0.25\ \mu A$ from Eq. (6). On the other hand, the apparent negative current to the beam collector is 1.0 μA ~ 5.0 μA. That is, the discrepancy ratio (I^-/I_i^-) is 10 ~ 20. We consider that this discrepancy between the net current I_i^- and the apparent current I^- is due to the negative current of the secondary

electrons generated by the $\mathring{\mu}^-$ particles through the gas ionization or the impacts with the beam collector surface.

Inversely, we can consider that a very weak generation of $\mathring{\mu}^-$ particle by a small power of the low energy electron beam, is observed clearly from the multiplied apparent current.

To explain the experimental results for the beam collector bias voltages V_S in Fig. 7 and Fig. 8, we assume that a negative muonlike particle $\mathring{\mu}^-$ decays into many secondary electrons on the surface of the beam collector. That is, the relation is given by

$$\mathring{\mu}^- \longrightarrow \mathrm{Ne}, \quad \text{..... (7)}$$

where e shows a secondary electron and N is the number of the electrons. Moreover, we assume that the energies of the secondary electrons are distributed from a few 10 eV to V_E (= 2 V_A) eV, where V_A is the first electron beam acceleration voltage. On these assumptions, the beam collector bias voltage V_S is necessary for drawing back the secondary electrons to the beam collector. Then, it is very important that the secondary electrons are produced in diffused positive ions or a secondary plasma as understood from Fig. 1 and Fig. 2, while the space charge effect of the secondary electrons does not appear.

In the second experimental apparatus (Fig. 11a), the mass analyzer body is biased negatively by V_B with respect to the electron gun anode and a discharge plasma of H_2 gas is used as a cathode supplying thermal electrons. Then, negative ions H^- of hydrogen[2] are accelerated together with electrons. Moreover, an extra anode with an additional electro-magnet is arranged. A weak magnetic field by the additional electro-magnet is applied perpendicularly to the electron beam, which is useful to focus the electron beam in the entrance slit and to absorb back ground electrons (which are generated through gas ionization by the electron beam and have low energies). That is, an electron beam with a monochromatic energy is injected into the mass analyzer by the extra anode.

A dependence of the beam collector current on the magnetic field of the mass analyzer, is determined in Fig. 11b under a bias potential $V_B \approx -200$V (7 in Fig. 11a). This bias potential V_B is applied in order to inject an positive ion beam into the mass analyzer, while the electron beam energy corresponding to the electron gun anode voltage V_A, is reduced by the

difference voltage ($V_A - |V_B|$) = 2000V – 200V. Thus, under the analyzing curvature radius r = 4.3 cm, the first peak of the beam collector current appears at a magnetic field 32.5 gauss of the mass analyzer, which is generated by the electron beam. The second peak also appears at a magnetic field 14 times larger than that of the first peak, which is considered to be generated by the $\mathring{\mu}^-$ beam. Besides the second peak, the third peak appears at a magnetic field 43 times larger than that of the first peak and 3 times larger than that of the second peak, which is obviously generated by the negative ion H^- of hydrogen. As a result of this experiment, it is more clearly proved that the second peak is generated by a negative muonlike particle which has a mass of about 1/9 times of hydrogen atom. If a discharge of helium He or argon Ar gas is used, the third peak does not appear while the first and second peaks appear.

In the above experimental method (as shown in Fig. 11a) where the mass analyzer body is biased by a negative voltage V_B with respect to the electron gun anode, we find that the following relations at their peaks of the beam collector current, are satisfied by, for electron,

$$r = \frac{3.4\sqrt{V_E}}{B_M}$$

$$V_E = V_A - |V_B|, \quad \text{..... (8)}$$

for negative muonlike particle,

$$r = \frac{48\sqrt{V_E}}{B_M}$$

$$V_E = V_A - |V_B|, \quad \text{..... (9)}$$

for negative hydrogen ion H^-,

$$r = \frac{144\sqrt{V_E}}{B_M}$$

$$V_E = V_A - |V_B|, \quad \text{..... (10)}$$

where V_E is an effective acceleration voltage in V (volt) unit, r is the analyzing curvature radius (= 4.3 cm) and B_M is the analyzing magnetic field (in gauss).

Here, the positive bias voltage V_S of the beam collector is determined by $|V_B|$ from the negative bias voltage V_B of the mass analyzer, as understood from 7 in Fig. 11a.

If the decelerator D in Fig. 1 (first experiment) is connected to the electron gun anode A or if the mass analyzer body in Fig. 11a (second experiment) is connected directly to the anode A (that is, $V_B = 0$), the peak of the negative beam collector current Γ corresponding to the negative muonlike particle, does not appear. That is, the negative muonlike peak in the mass analysis is not produced for the injection of only the electron beam. Similarly, when the negative bias voltage V_B of the mass analyzer body approaches to $-|V_A|$ (V_A is the electron gun anode voltage) and the electron beam is repelled electrically, the negative muonlike peak disappears. That is, the negative muonlike peak is not produced also for the injection of only the ion beam. Thus, we can consider that the injection of an electron beam accompanying an ion beam is a necessary condition to produce the negative muonlike peak. Moreover, the first experiment (in Fig. 1) where the injected ion beam is stopped electrically in the region of cyclotron motions of the reaccelerated electrons, is very efficient because (1) the negative muonlike particle energy is determined exactly by twice of an acceleration voltage of an initial electron beam, (2) the mechanical accuracy of electron beam injection through the entrance slit into the mass analyzer, is relaxed (while the arrangement of electron gun becomes very easy), and (3) a back ground or noisy electron current becomes very small for the detection of negative muonlike current.

From these experimental confirmations, the secondary electron current peak at the negative muonlike position on the mass analysis can be related with an interaction between the bunched beam electrons (due to the local cyclotron motions) and the positive ion beam (in the second experimental apparatus) or the electrically stopped beam ions (in the first experimental apparatus). In conclusion, we may expect from the peak of secondary electron current at the exact position of negative muon in the magnetic mass analysis system, that a very small amount of negative muon is produced by the injection of a low energy electron beam accompanying an ion beam, through the negative muon is not detected directly.

References

1. L.W. Alvarez et al.: *Phys. Rev.* **105** (1957) 1127.
2. M. Bacal and G.W. Hamilton: *Phys. Rev. Lett.* **42** (1979) 1538.

Fig. 1 and Fig. 2: Schematic diagrams of the first experimental apparatus.

F: Filament as electron emitter. K: Cathode of electron gun. A: Anode of electron gun. V_A: Initial electron acceleration voltage. I_A: Total negative current. F.E.B.: First electron beam. G: Neutral gas. D: Decelerator of F.E.B. S: Entrance slit (3 mm × 10 mm). Ins: Insulator. I.B.: Ion beam. S.E.B.: Second electron beam. e: Electrons with cyclotron motions. $\mathring{\mu}^-$: Negative muonlike particle. (M.A.): Mass analyzer. Fe: Iron. C: Magnetic Coil. (N): North pole of electro-magnet. (S): South pole. B_M: Analyzing magnetic field. B.C.: Beam collector. Γ^-: Negative current to B.C. V_S: Bias voltage of B.C. with respect to mass analyzer body. S.P.: Secondary plasma inside (M.A.). X: End of uniform magnetic field.

Fig. 3 Fringe magnetic field distribution.

B_M: Analyzing magnetic field of (M.A.). B_O: Uniform magnetic field inside (M.A.). X: End of uniform magnetic field. S: Entrance slit position. Fe: Magnetic field distribution in a case using iron plate as D in Fig. 1. Cu: Magnetic field distribution in a case using copper plate as D in Fig. 1.

Fig. 4 Dependences of the negative beam collector current Γ^- on the analyzing magnetic field B_M under various initial electron acceleration voltages V_A. The positive beam collector bias voltage V_S = 100V.

(1): V_A = 100V. (2): V_A = 200V. (3): V_A = 400V. (4): V_A = 800V. (5): V_A = 1200V.

The neutral gas pressure (air) is 5×10^{-6} Torr in the first electron beam region. $\mathring{\mu}^-$: (means negative muonlike particle). The total anode current I_A = 1.8 mA.

Fig. 5 Comparisons between $\mathring{\mu}^-$ and H^- characteristics while H_2 gas is introduced into the first electron beam region at a pressure of 3×10^{-4} Torr. The positive beam collector bias V_S = 100V. The total anode current I_A = 1.0 mA.

(1): V_A = 100V. (2): V_A = 200V. (3): V_A = 300V.

The pressure in the electron gun cathode region is 1×10^{-5} Torr.

Fig. 6 Dependences of Γ^- on B_M under various V_A while He gas is introduced into the first electron beam region at a pressure of 1.5×10^{-4} Torr. The positive beam collector bias voltage V_S = 100V. The total anode current I_A = 1 mA.
(1): V_A = 100V. (2): V_A = 200V. (3): V_A = 400V. (4): V_A = 800V. (5): V_A = 1200V.
The pressure in the electron gun cathode region is 1×10^{-5} Torr.

Fig. 7 Dependences of Γ^- on B_M under various bias voltages V_S of the beam collector at V_A = 200V.
(1): V_S = 50V. (2): V_S = 100V. (3): V_S = 200V. (4): V_S = 400V. (5): V_S = 300V. (6): V_S = 500V.
Total current to electron gun anode I_A = 1.8 mA. Pressure in F.E.B. = 5×10^{-6} Torr.

Fig. 8 Dependences of Γ^- on B_M under various V_S at V_A = 1200V.
(1): V_S = 100V. (2): V_S = 200V. (3): V_S = 400V. (4): V_S = 600V. (5): V_S = 1200V.
I_A = 1.8 mA. Pressure in F.E.B. = 5×10^{-6} Torr.

Fig. 9 Dependences of Γ^- on B_M under various total current I_A to electron gun anode at V_A = 400V and V_S = 350V, and pressure in F.E.B. = 5×10^{-6} Torr.
(1): I_A = 2 mA. (2): I_A = 4 mA. (3): I_A = 6 mA. (4): I_A = 8 mA.

Fig. 10 Dependences of Γ^- on B_M under various pressure P of Ar gas in the first electron beam region at V_A = 400V, V_S = 350V and I_A = 3 mA.
(1): P = 5×10^{-6} Torr. (2): P = 5×10^{-5} Torr. (3): P = 1×10^{-4} Torr. (4): P = 2×10^{-4} Torr.

Fig. 11 Schematic diagram of the second experimental apparatus (a) and experimental result of mass analysis (b). a; 1: Anode and cathode for H_2 gas discharge. 2: Anode for accelerating electrons and H^- ions produced by H_2 gas discharge. 3: Acceleration voltage of 2000V for electrons and H^- ions. 4: Electron beam and H^- ion beam. 5: Magnetic coil. 6: Intermediate electrode. 7: Bias voltage of the mass analyzer with respect to anode (–200V). 8: Extra anode to guide the electron beam and H^- ion beam for the mass analyzer. 9: Magnetic field for mass analysis. 10: Hydrogen gas H_2 introduced into the discharge region. 11: Discharge plasma. 12: Ammeter for the beam corrector. 13: Mass analyzer. 14: Beam collector. b; Dependence of beam collector current on analyzing magnetic field under a bias voltage $V_B = -200V$. e: Electron current. $\mathring{\mu}^-$: Negative muonlike current. H^-: Hydrogen negative ion current. B_M: Strength of magnetic field. I_e: Scale for electron current e. I^-: Scale for $\mathring{\mu}^-$ and H^- current. Pressures of H_2 gas are 3×10^{-4} Torr in the discharge region and 2×10^{-5} Torr in the electron beam region.

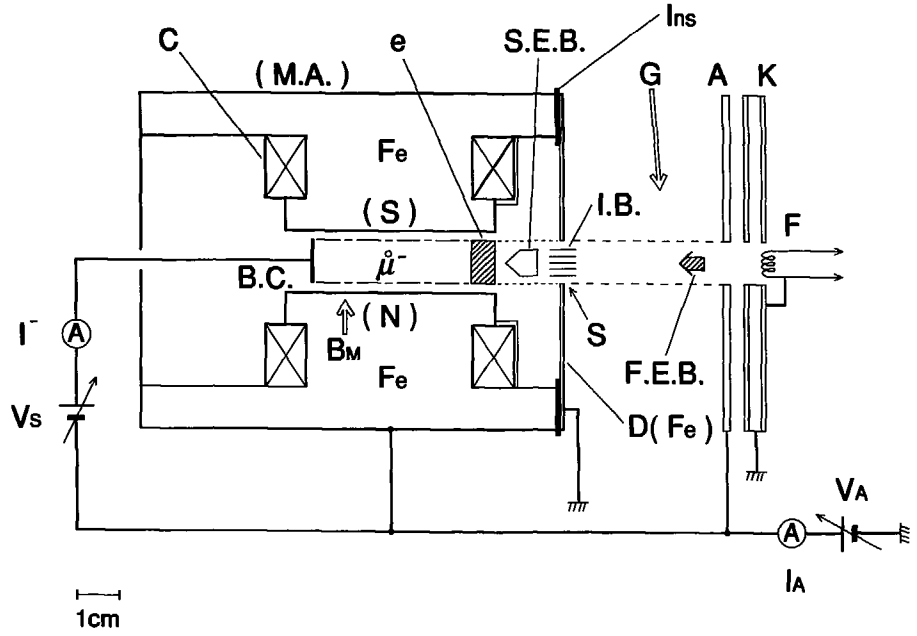

Fig. 1

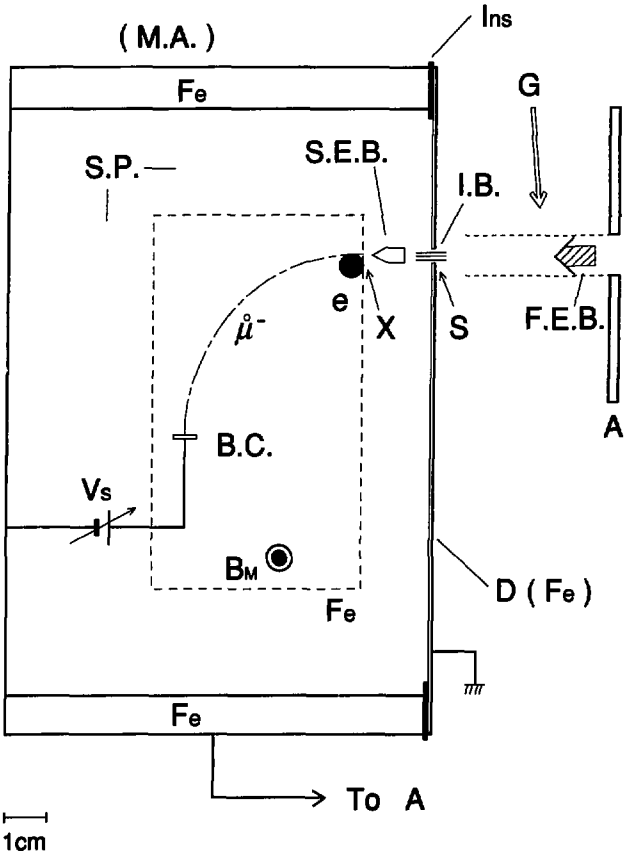

Fig. 2

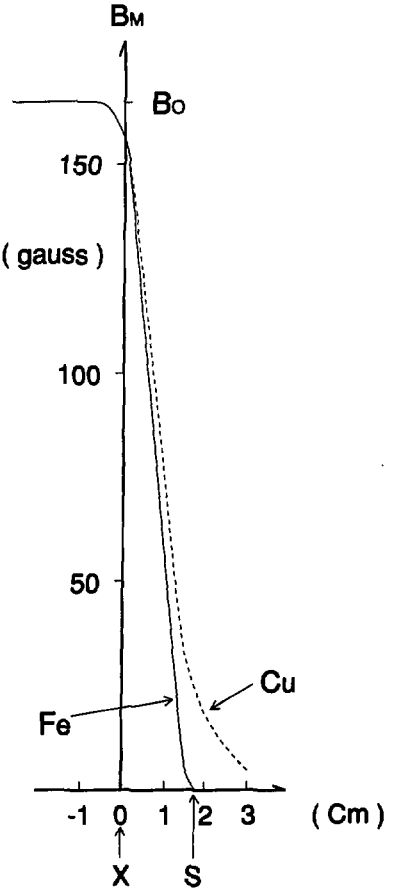

Fig. 3

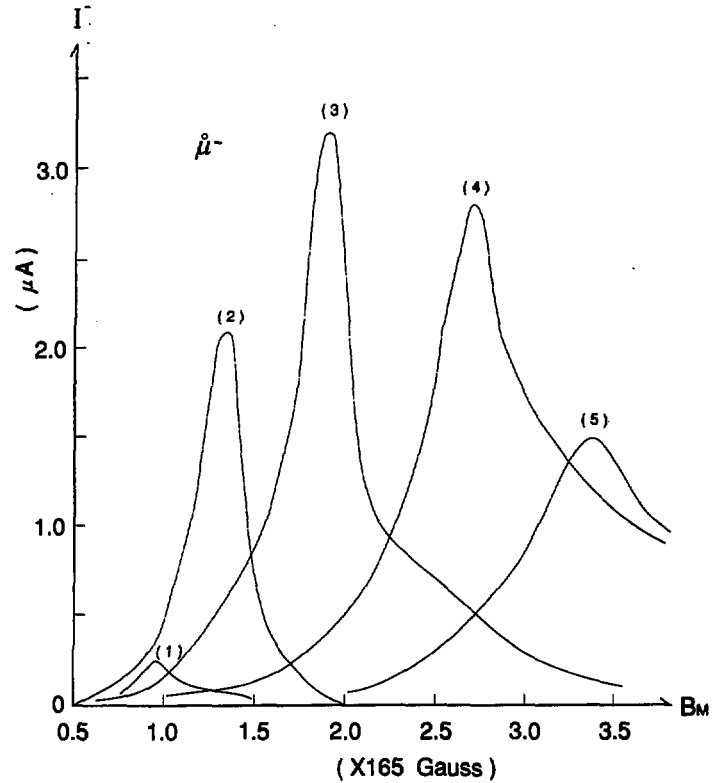

Fig. 4

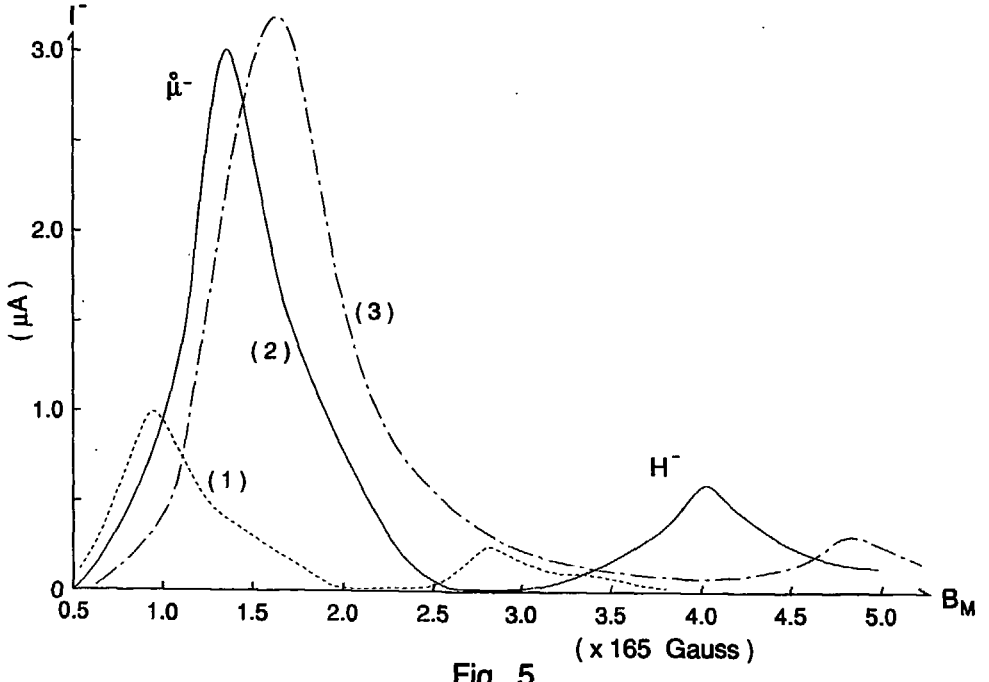

Fig . 5

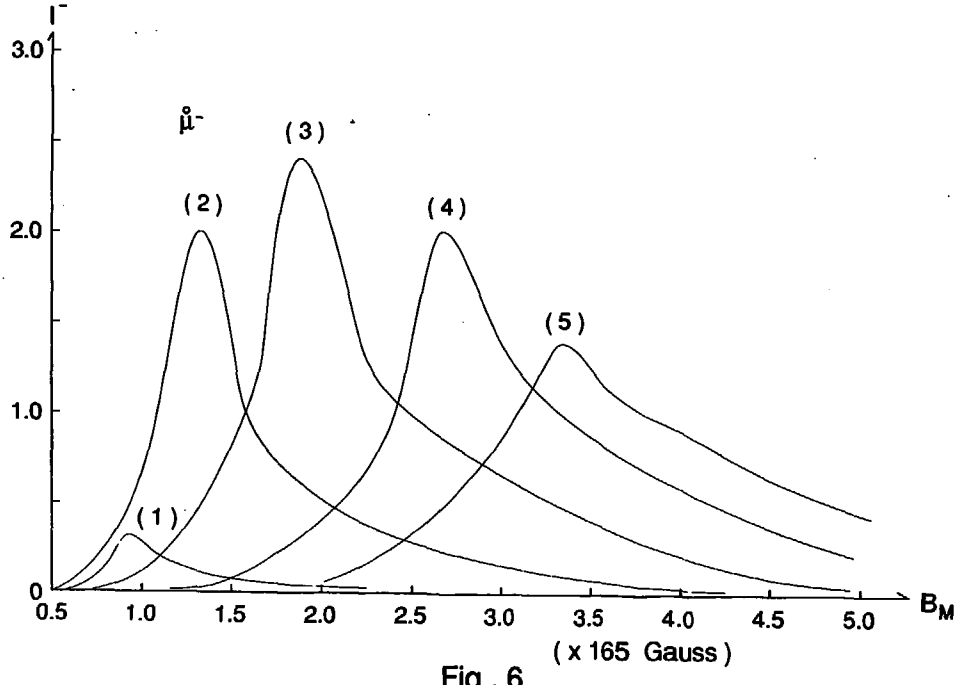

Fig . 6

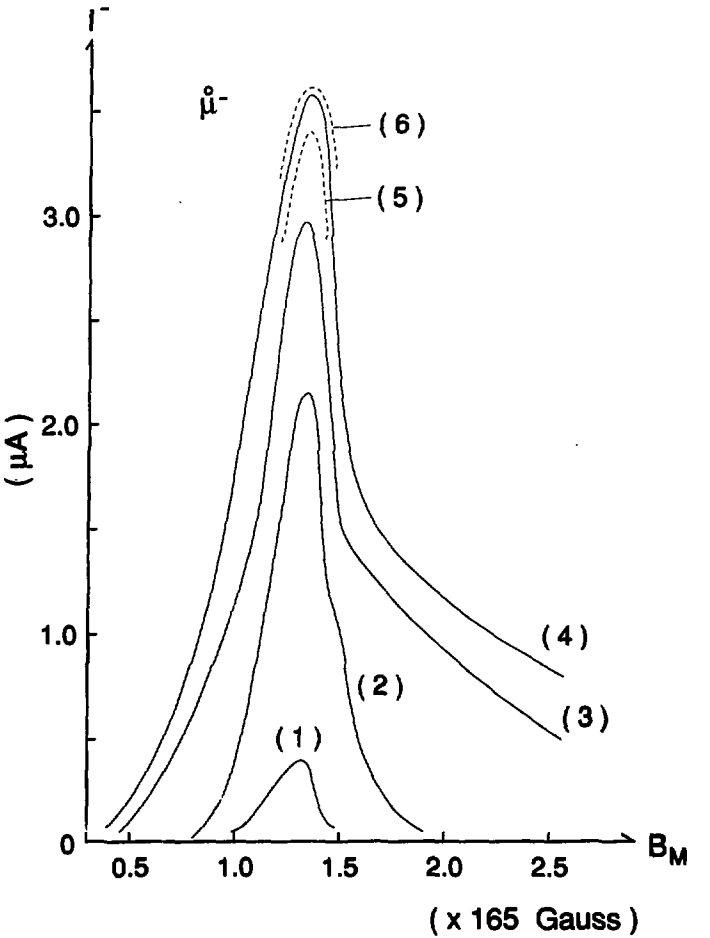

Fig . 7

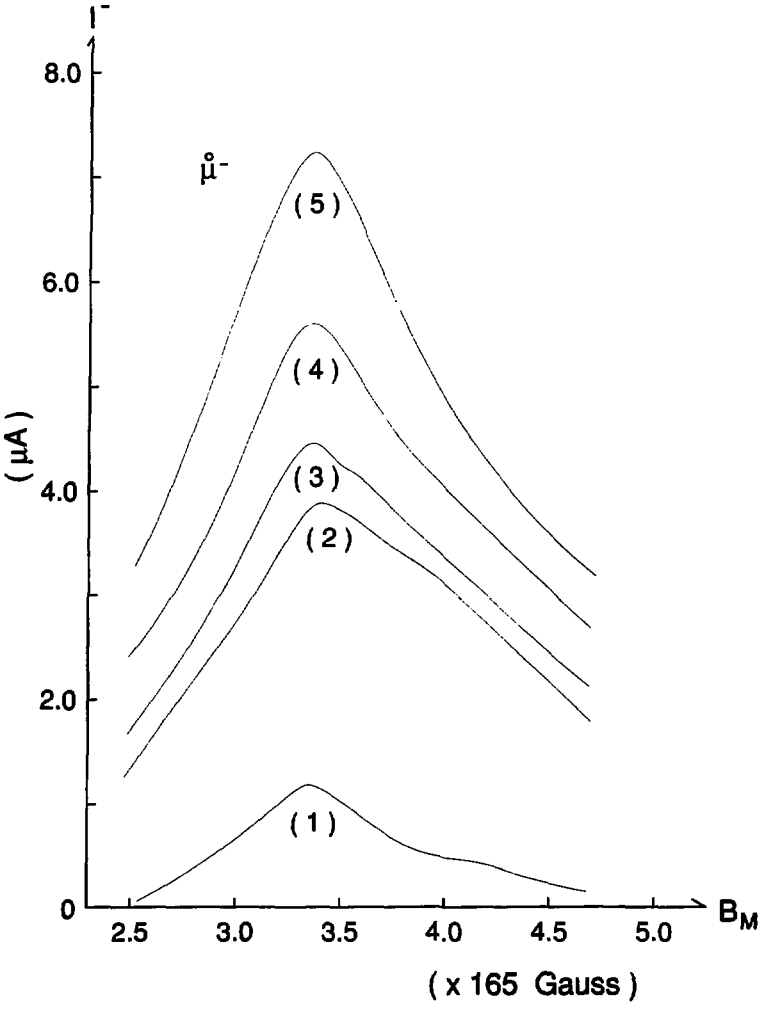

Fig . 8

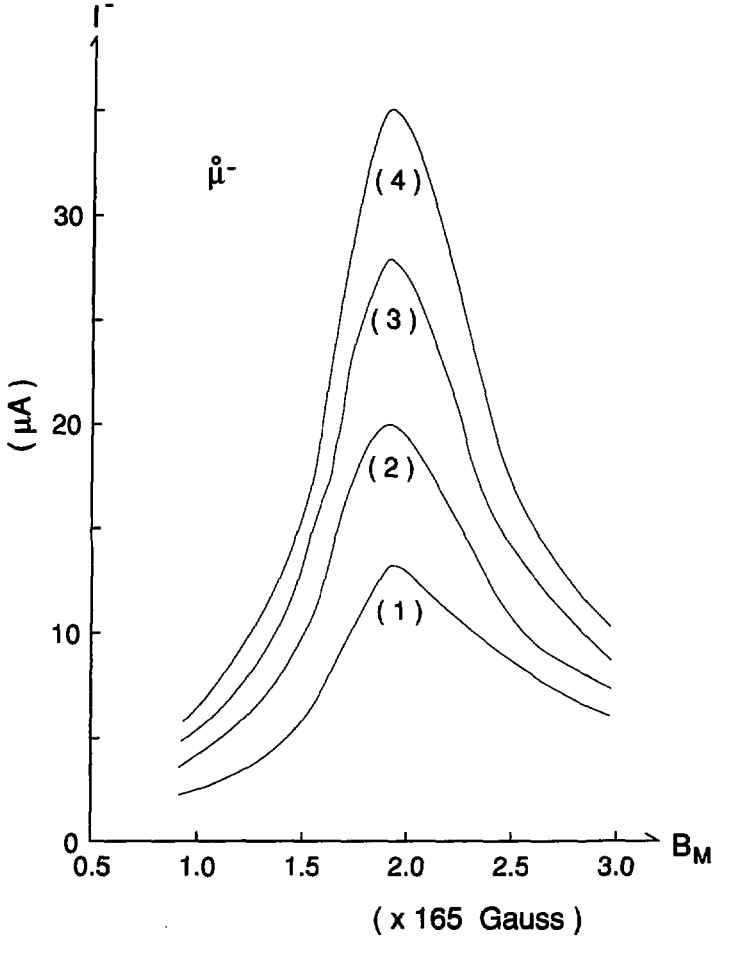

Fig . 9

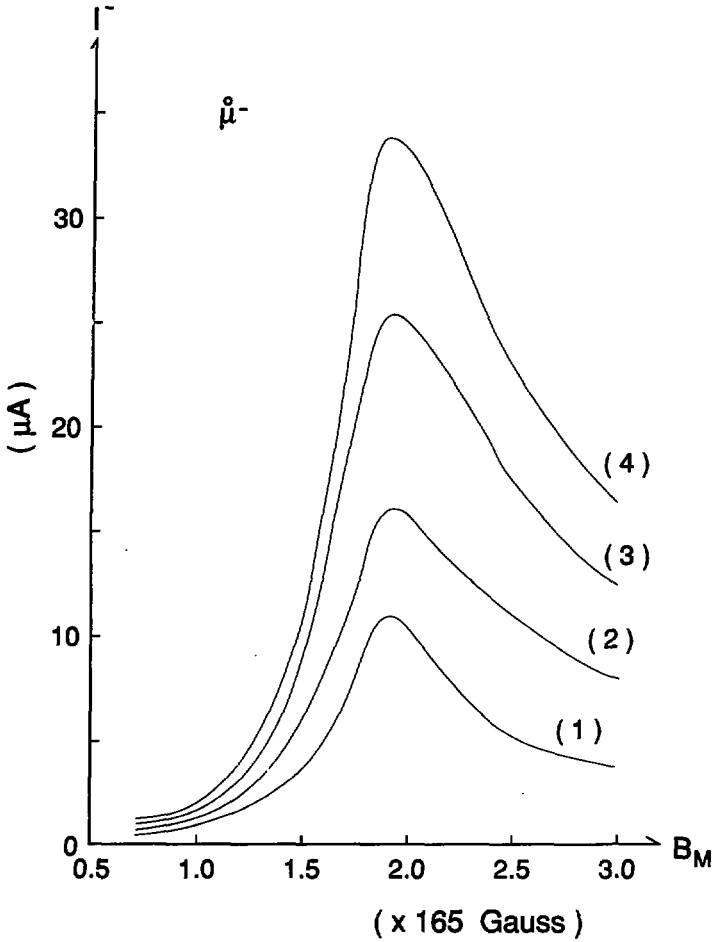

Fig . 10

a

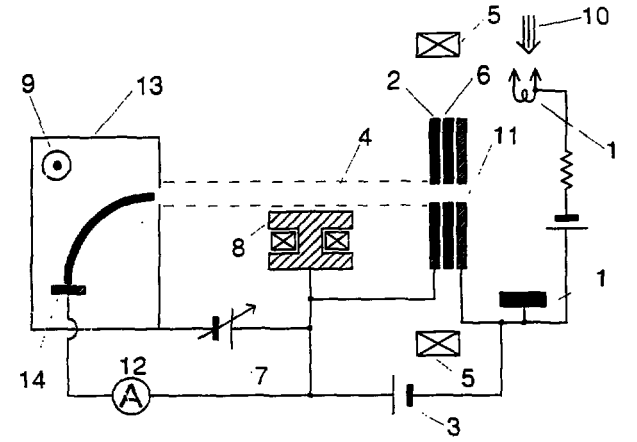
5
10
9
13
2
6
4
11
1
8
1
14
12
7
5
3

b

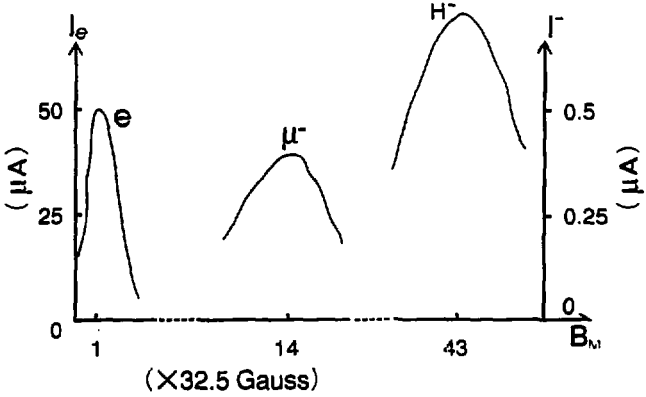
I_e
H⁻
I⁻
50
e
μ⁻
0.5
(μA)
25
0.25
(μA)
0
0
1
14
43
B_M
(×32.5 Gauss)

Fig.11

Appendix I

As a reference, we show a most simple experimental apparatus (A. Fig. 1). There, an electron beam of 2000 eV in a diameter of 10 mm is generated by an electron gun where a weak magnetic field of 20 gauss is applied. A part (a few 100 μA) of this electron beam is injected into the mass analyzer through the entrance slit. A neutral gas (air) is introduced in the electron beam region where a pressure of the gas is 4×10^{-5} Torr. (The pressure in the cathode region of the electron gun is kept below 4×10^{-6} Torr).

A dependence of the beam collector current on the magnetic field of the mass analyzer is determined (A. Fig. 2). The first peak of the negative current to the beam collector appears at a magnetic field 23 gauss, which corresponds to the injected electron beam energy. As this energy of electron beam is determined to be near 1000 eV, the electron beam is decelerated by the negative bias voltage near the slit of the mass analyzer. Then, the positive ions produced by introducing the neutral gas, are accelerated at the bias voltage $|V_B| \approx 1000V$. The second peak of the negative current appears at a magnetic field 322 gauss which is about 14 times larger than that of the first peak. For the above experiment, the fundamental principle is shown in A. Fig. 3.

As another reference, a new mass analyzer is set to change the analyzing radius r. Two iron cores of the new mass analyzer for the magnetic field B_M are wide in area (9 cm × 7 cm) in comparison with the previous mass analyzer (9 cm × 5 cm). Thus, the analyzing radius r is varied from 3.0 cm to 8.5 cm in four steps under an initial electron beam acceleration voltage 1500V (3 in A. Fig. 1) and an negative bias voltage −1000V (7 in A. Fig. 1). In A. Fig. 4, four dependences of the second particle ($\mathring{\mu}^-$) current to the beam collector, on the magnetic field B_M are shown for $r = 3.0$ cm, $r \approx 4.25$ cm, $r = 6.0$ cm and $r = 8.5$ cm (45°). We can find from A. Fig. 4 that each peak of the second particle current appears when the Eq. (9) is exactly satisfied if the injected electron beam energy is determined by the difference voltage (1500V − 1000V) 500V.

A. Fig. 1 Schematic diagram of the first experimental apparatus (a) and mass analysis method by electro-magnet (b).
1: W filament cathode which emits thermal electrons. 2: Anode for accelerating electrons. 3: Acceleration voltage (2000V) for electrons. 4: Electron beam. 5: Magnetic coil to produce magnetic field in the region where electrons are accelerated. 6: Intermediate electrode for electron acceleration. 7: Bias voltage of electro-magnet system with respect to anode accelerating electrons. 8: Iron. 9: Magnetic field. 10: Magnetic coil. 11: Metal plate with slit. 12: Introduced neutral gas. 13: Mass analysis system by magnetic field. 14: Collector for beam current. 15: Ammeter. An electron gun is formed by (1, 2, 3, 5, 6) and an electron beam (4) is produced. An electro-magnet system to inject the electron beam is formed by (8, 10, 11). A mass analysis is performed by (9, 15). Positive ions in the electron beam are produced by introducing neutral gas (12).

A. Fig. 2 Dependences of beam collector current on analyzing magnetic field (9 in A. Fig. 1). e: Electron current. $\mathring{\mu}^-$: Negative muonlike current. B_M: Strength of analyzing magnetic field. I_e: Scale for electron current e. I^-: Scale for an apparent current of $\mathring{\mu}^-$. Solid lines show a case of mass analysis under a pressure of 4×10^{-5} Torr by introducing a neutral gas (air) in the electron beam. Dotted lines show a fundamental case under a base pressure of 4×10^{-6} Torr.

A. Fig. 3 Fundamental Schematic Diagram of $\mathring{\mu}^-$ Production.
$\mathring{\mu}^-$: Negative Muonlike Particle. e: Electron Bunch. B: Uniform Magnetic Field. M.A.: Mass Analyzer. A: Electron Gun Anode. K: Electron Gun Cathode. E.B.: Electron Beam. I.B.: Ion Beam. B.C.: Beam Collector. G: Neutral Gas. V_S: Potential to draw back Secondary Electrons. S.P.: Secondary Plasma.

A. Fig. 4 Relations between analyzing magnetic field B_M and curvature radius r in mass analyses, when each negative current I^- of second particle ($\mathring{\mu}^-$: negative muonlike particle) to beam collector (14 in A. Fig. 1) shows a peak.
(1) r = 3.0 cm. (2) r = 4.25 cm. (3) r = 6.0 cm. (4) r = 8.5 cm (45°).
Acceleration voltage of electron beam (3 in A. Fig. 1): 1500V. Negative bias voltage (7 in A. Fig. 1): −1000V. Neutral gas pressures: 1×10^{-4} Torr in electron beam region and 1×10^{-5} Torr in electron gun cathode region. Distance between electron gun and mass analyzer: 8.5 cm. Parallel magnetic field (5 in A. Fig. 1) is not applied.

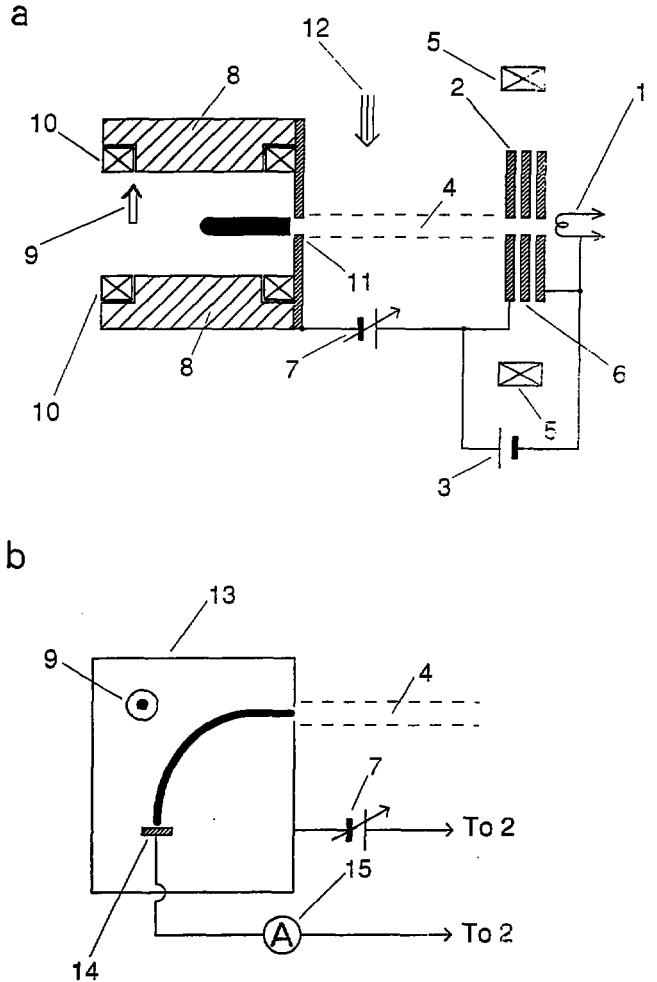

A. Fig. 1

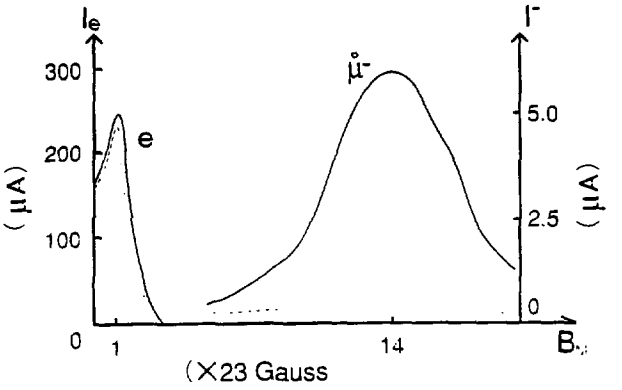

A. Fig. 2

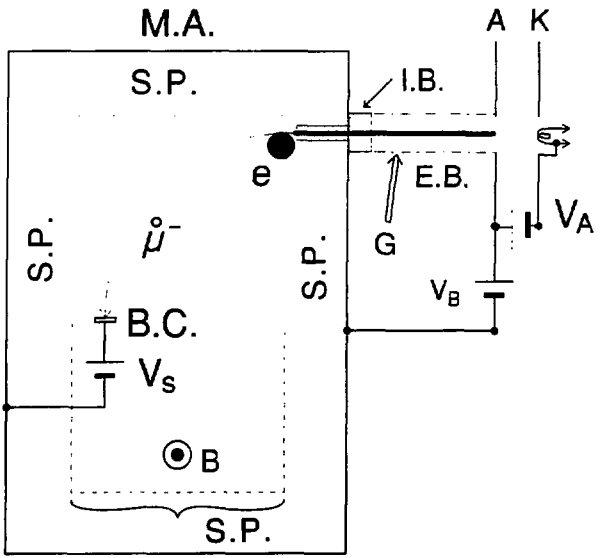

A. Fig. 3

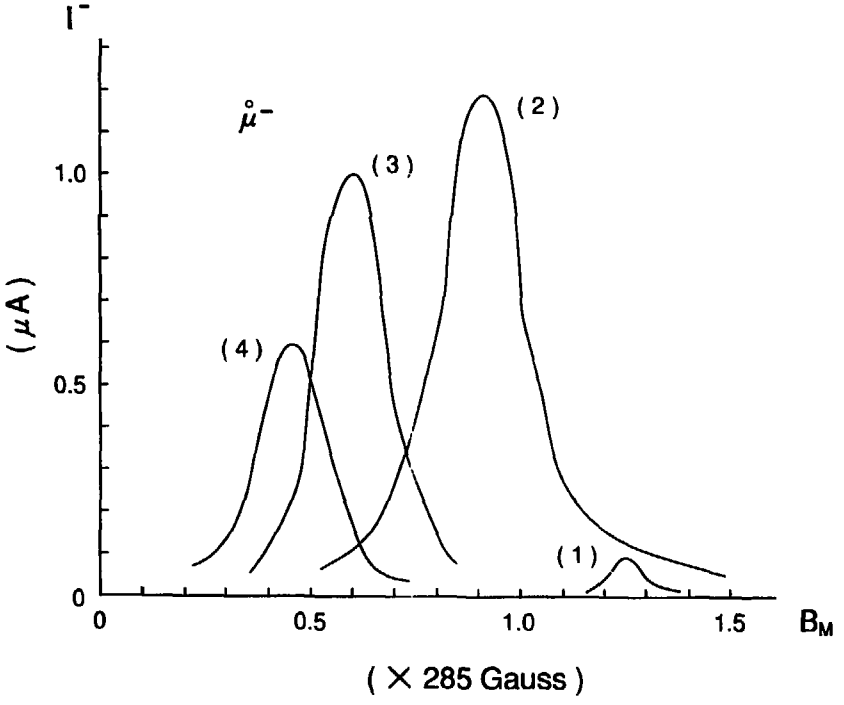

A. Fig. 4

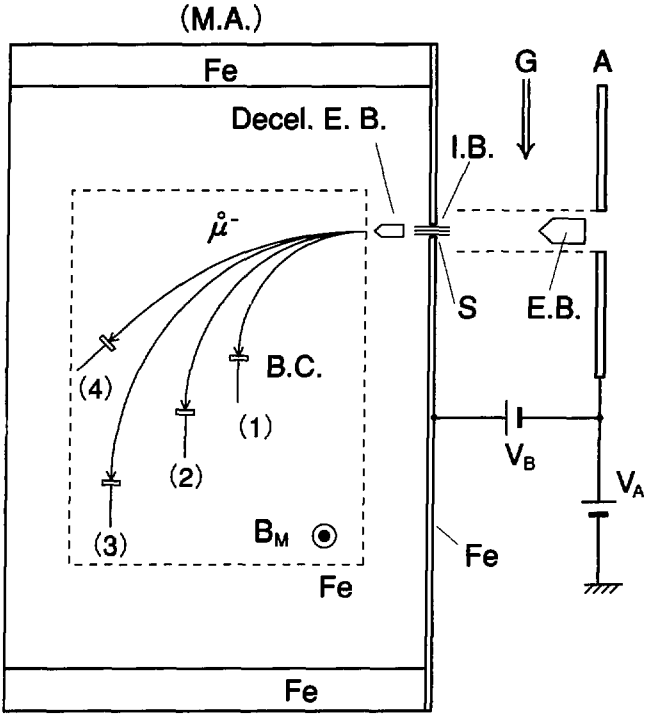

A. Fig. 4'

Appendix II

— Two kinds of coherent interaction between electrons and positive ions —

At the CERN Symposium in 1956, V.I. Veksler proposed a coherent interaction for a bunch of positive ions in an electron beam as a possibility of effective ion acceleration.[1] According to the coherent interaction theory, the bunch of positive ions with a charge number N will be accelerated through an energy loss of the electron beam, by N^2 times largely in comparison with a case of single positive ion in the electron beam. As a result, each positive ion in the bunch will be accelerated by N times largely. The experimental conception can be shown as A. Fig. X (1). However, we can not expect the coherent interaction between a bunch of positive ions and an electron beam. Because the bunched ions diffuse easily along the electron beam and become unstable even if the electron beam is stabilized by the parallel magnetic field.

Inversely, in this paper, we considered another coherent interaction for a bunch of electrons in a positive ion beam. First, a positive ion beam and an electron beam are injected perpendicularly to a weak magnetic field. Next, we adjust the weak magnetic field in the following condition. That is, the weak magnetic field is effective for only the electron beam (a very small cyclotron radius below a radius of the ion beam) and is not effective for the ion beam (a very large cyclotron radius). This experimental conception can be shown as A. Fig. X(2). Then, we find that the electron beam changes into a small bunch of energetic electrons through multiple cyclotron motions in a small radius, while the positive ion beam moves straight almost. Thus, the bunch of electrons in the ion beam, is stabilized by the weak and perpendicular magnetic field.

Here, we can consider a new coherent interaction between the bunch of electrons and the positive ion beam: As the bunch of electrons can not move along the positive ion beam because of the perpendicular magnetic field, an internal energy of the electron bunch increases extremely through an energy transfer from the ion beam. In this process, we may expect a "high energy resonance state" of the electron bunch which produces negative muons.

Reference

1) V.I. Veksler: *CERN Symposium* **1** (1956) 80.

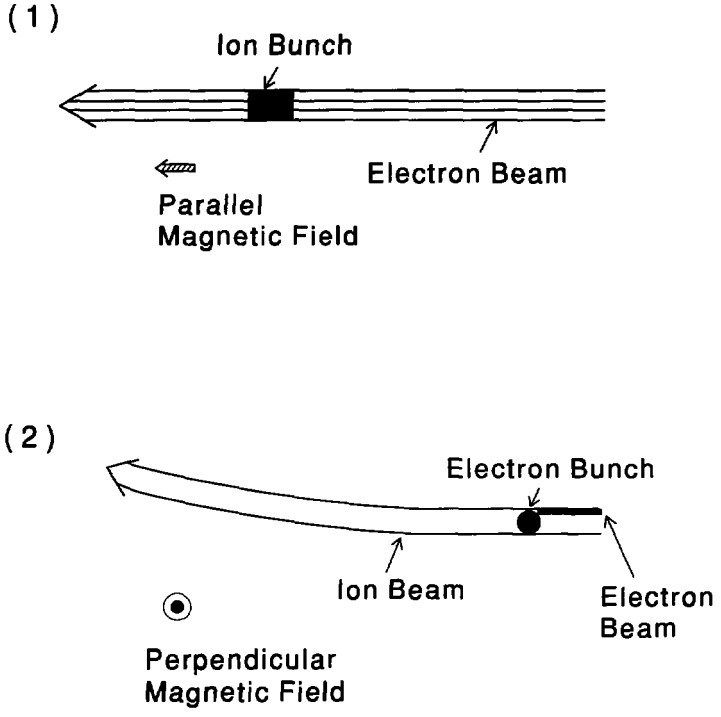
(1)
Ion Bunch
Electron Beam
Parallel
Magnetic Field
(2)
Electron Bunch
Ion Beam
Electron
Beam
Perpendicular
Magnetic Field

Fig. X

Recent Issues of NIFS Series

NIFS-216 M. Yagi, K. Itoh, S.-I. Itoh, A. Fukuyama and M. Azumi, *Analysis of Current Diffusive Ballooning Mode*; Apr. 1993

NIFS-217 J. Guasp, K. Yamazaki and O. Motojima, *Particle Orbit Analysis for LHD Helical Axis Configurations* ; Apr. 1993

NIFS-218 T. Yabe, T. Ito and M. Okazaki, *Holography Machine HORN-1 for Computer-aided Retrieve of Virtual Three-dimensional Image* ; Apr. 1993

NIFS-219 K. Itoh, S.-I. Itoh, A. Fukuyama, M. Yagi and M. Azumi, *Self-sustained Turbulence and L-Mode Confinement in Toroidal Plasmas* ; Apr. 1993

NIFS-220 T. Watari, R. Kumazawa, T. Mutoh, T. Seki, K. Nishimura and F. Shimpo, *Applications of Non-resonant RF Forces to Improvement of Tokamak Reactor Performances Part I: Application of Ponderomotive Force* ; May 1993

NIFS-221 S.-I. Itoh, K. Itoh, and A. Fukuyama, *ELMy-H mode as Limit Cycle and Transient Responses of H-modes in Tokamaks* ; May 1993

NIFS-222 H. Hojo, M. Inutake, M. Ichimura, R. Katsumata and T. Watanabe, *Interchange Stability Criteria for Anisotropic Central-Cell Plasmas in the Tandem Mirror GAMMA 10* ; May 1993

NIFS-223 K. Itoh, S.-I. Itoh, M. Yagi, A. Fukuyama and M. Azumi, *Theory of Pseudo-Classical Confinement and Transmutation to L-Mode;* May 1993

NIFS-224 M. Tanaka, *HIDENEK: An Implicit Particle Simulation of Kinetic-MHD Phenomena in Three-Dimensional Plasmas;* May 1993

NIFS-225 H. Hojo and T. Hatori, *Bounce Resonance Heating and Transport in a Magnetic Mirror;* May 1993

NIFS-226 S.-I. Itoh, K. Itoh, A. Fukuyama, M. Yagi, *Theory of Anomalous Transport in H-Mode Plasmas;* May 1993

NIFS-227 T. Yamagishi, *Anomalous Cross Field Flux in CHS* ; May 1993

NIFS-228 Y. Ohkouchi, S. Sasaki, S. Takamura, T. Kato, *Effective Emission and Ionization Rate Coefficients of Atomic Carbons in Plasmas;* June 1993

NIFS-229 K. Itoh, M. Yagi, A. Fukuyama, S.-I. Itoh and M. Azumi, *Comment on*

'A Mean Field Ohm's Law for Collisionless Plasmas; June 1993

NIFS-230 H. Idei, K. Ida, H. Sanuki, H. Yamada, H. Iguchi, S. Kubo, R. Akiyama, H. Arimoto, M. Fujiwara, M. Hosokawa, K. Matsuoka, S. Morita, K. Nishimura, K. Ohkubo, S. Okamura, S. Sakakibara, C. Takahashi, Y. Takita, K. Tsumori and I. Yamada, *Transition of Radial Electric Field by Electron Cyclotron Heating in Stellarator Plasmas;* June 1993

NIFS-231 H.J. Gardner and K. Ichiguchi, *Free-Boundary Equilibrium Studies for the Large Helical Device,* June 1993

NIFS-232 K. Itoh, S.-I. Itoh, A. Fukuyama, H. Sanuki and M. Yagi, *Confinement Improvement in H-Mode-Like Plasmas in Helical Systems,* June 1993

NIFS-233 R. Horiuchi and T. Sato, *Collisionless Driven Magnetic Reconnection,* June 1993

NIFS-234 K. Itoh, S.-I. Itoh, A. Fukuyama, M. Yagi and M. *Azumi, Prandtl Number of Toroidal Plasmas;* June 1993

NIFS-235 S. Kawata, S. Kato and S. Kiyokawa , *Screening Constants for Plasma;* June 1993

NIFS-236 A. Fujisawa and Y. Hamada, *Theoretical Study of Cylindrical Energy Analyzers for MeV Range Heavy Ion Beam Probes;* July 1993

NIFS-237 N. Ohyabu, A. Sagara, T. Ono, T. Kawamura and O. Motojima, *Carbon Sheet Pumping;* July 1993

NIFS-238 K. Watanabe, T. Sato and Y. Nakayama, *Q-profile Flattening due to Nonlinear Development of Resistive Kink Mode and Ensuing Fast Crash in Sawtooth Oscillations;* July 1993

NIFS-239 N. Ohyabu, T. Watanabe, Hantao Ji, H. Akao, T. Ono, T. Kawamura, K. Yamazaki, K. Akaishi, N. Inoue, A. Komori, Y. Kubota, N. Noda, A. Sagara, H. Suzuki, O. Motojima, M. Fujiwara, A. Iiyoshi, *LHD Helical Divertor;* July 1993

NIFS-240 Y. Miura, F. Okano, N. Suzuki, M. Mori, K. Hoshino, H. Maeda, T. Takizuka, JFT-2M Group, K. Itoh and S.-I. Itoh, *Ion Heat Pulse after Sawtooth Crash in the JFT-2M Tokamak;* Aug. 1993

NIFS-241 K. Ida, Y.Miura, T. Matsuda, K. Itoh and JFT-2M Group, *Observation of non Diffusive Term of Toroidal Momentum Transport in the JFT-2M Tokamak;* Aug. 1993

NIFS-242 O.J.W.F. Kardaun, S.-I. Itoh, K. Itoh and J.W.P.F. Kardaun, *Discriminant Analysis to Predict the Occurrence of ELMS in H-*

Mode Discharges; Aug. 1993

NIFS-243 K. Itoh, S.-I. Itoh, A. Fukuyama,
Modelling of Transport Phenomena; Sep. 1993

NIFS-244 J. Todoroki,
Averaged Resistive MHD Equations; Sep. 1993

NIFS-245 M. Tanaka,
The Origin of Collisionless Dissipation in Magnetic Reconnection; Sep. 1993

NIFS-246 M. Yagi, K. Itoh, S.-I. Itoh, A. Fukuyama and M. Azumi,
Current Diffusive Ballooning Mode in Seecond Stability Region of Tokamaks; Sep. 1993

NIFS-247 T. Yamagishi,
Trapped Electron Instabilities due to Electron Temperature Gradient and Anomalous Transport; Oct. 1993

NIFS-248 Y. Kondoh,
Attractors of Dissipative Structure in Three Disspative Fluids; Oct. 1993

NIFS-249 S. Murakami, M. Okamoto, N. Nakajima, M. Ohnishi, H. Okada,
Monte Carlo Simulation Study of the ICRF Minority Heating in the Large Helical Device; Oct. 1993

NIFS-250 A. Iiyoshi, H. Momota, O. Motojima, M. Okamoto, S. Sudo, Y. Tomita, S. Yamaguchi, M. Ohnishi, M. Onozuka, C. Uenosono,
Innovative Energy Production in Fusion Reactors; Oct. 1993

NIFS-251 H. Momota, O. Motojima, M. Okamoto, S. Sudo, Y. Tomita, S. Yamaguchi, A. Iiyoshi, M. Onozuka, M. Ohnishi, C. Uenosono,
Characteristics of D-^{3}He Fueled FRC Reactor: ARTEMIS-L, Nov. 1993

NIFS-252 Y. Tomita, L.Y. Shu, H. Momota,
Direct Energy Conversion System for D-^{3}He Fusion, Nov. 1993

NIFS-253 S. Sudo, Y. Tomita, S. Yamaguchi, A. Iiyoshi, H. Momota, O. Motojima, M. Okamoto, M. Ohnishi, M. Onozuka, C. Uenosono,
Hydrogen Production in Fusion Reactors, Nov. 1993

NIFS-254 S. Yamaguchi, A. Iiyoshi, O. Motojima, M. Okamoto, S. Sudo, M. Ohnishi, M. Onozuka, C. Uenosono,
Direct Energy Conversion of Radiation Energy in Fusion Reactor, Nov. 1993

NIFS-255 S. Sudo, M. Kanno, H. Kaneko, S. Saka, T. Shirai, T. Baba,
Proposed High Speed Pellet Injection System "HIPEL" for Large Helical Device
Nov. 1993

NIFS-256 S. Yamada, H. Chikaraishi, S. Tanahashi, T. Mito, K. Takahata, N. Yanagi, M. Sakamoto, A. Nishimura, O. Motojima, J. Yamamoto, Y. Yonenaga, R. Watanabe,
Improvement of a High Current DC Power Supply System for Testing the Large Scaled Superconducting Cables and Magnets; Nov. 1993

NIFS-257 S. Sasaki, Y. Uesugi, S. Takamura, H. Sanuki, K. Kadota,
Temporal Behavior of the Electron Density Profile During Limiter Biasing in the HYBTOK-II Tokamak; Nov. 1993

NIFS-258 K. Yamazaki, H. Kaneko, S. Yamaguchi, K.Y. Watanabe, Y.Taniguchi, O.Motojima, LHD Group,
Design of Central Control System for Large Helical Device (LHD); Nov. 1993

NIFS-259 K. Yamazaki, H. Kaneko, S. Yamaguchi, K.Y. Watanabe, Y.Taniguchi, O.Motojima, LHD Group,
Design of Central Control System for Large Helical Device (LHD); Nov. 1993

NIFS-260 B.V.Kuteev,
Pellet Ablation in Large Helical Device; Nov. 1993

NIFS-261 K. Yamazaki,
Proposal of "MODULAR HELIOTRON': Advanced Modular Helical System Compatible with Closed Helical Divertor; Nov. 1993

NIFS-262 V.D.Pustovitov,
Some Theoretical Problems of Magnetic Diagnostics in Tokamaks and Stellarators; Dec. 1993

NIFS-263 A. Fujisawa, H. Iguchi, Y. Hamada
A Study of Non-Ideal Focus Properties of 30° Parallel Plate Energy Analyzers; Dec. 1993

NIFS-264 K. Masai,
Nonequilibria in Thermal Emission from Supernova Remnants; Dec. 1993

NIFS-265 K. Masai, K. Nomoto,
X-Ray Enhancement of SN 1987A Due to Interaction with its Ring-like Nebula; Dec. 1993